Nanoelectronics and Its New Materials – A NEW ERA OF NANOSCIENCE

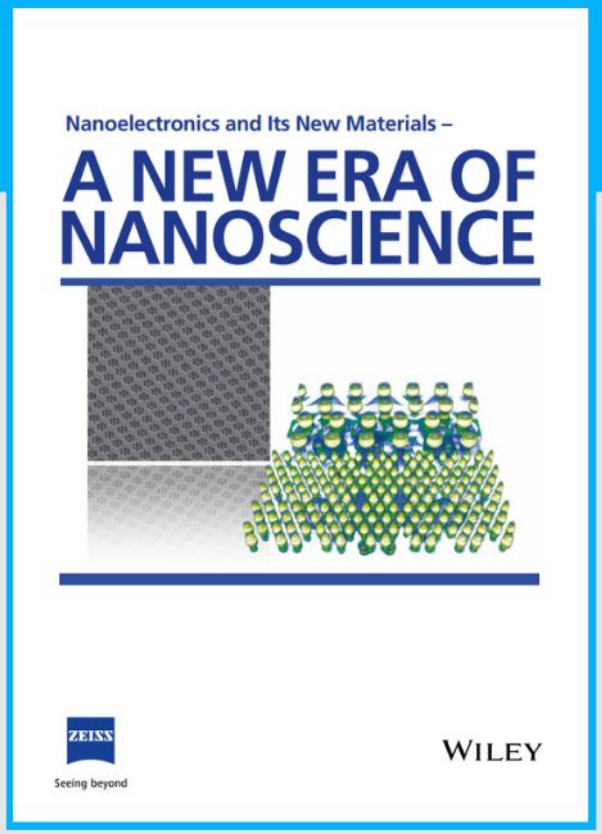

Discover the recent advances in electronics research and fundamental nanoscience.

Nanotechnology has become the driving force behind breakthroughs in engineering, materials science, physics, chemistry, and biological sciences. In this compendium, we delve into a wide range of novel applications that highlight recent advances in electronics research and fundamental nanoscience. From surface analysis and defect detection to tailored optical functionality and transparent nanowire electrodes, this eBook covers key topics that will revolutionize the future of electronics.

To get your hands on this valuable resource and unleash the power of nanotechnology, simply download the eBook now. Stay ahead of the curve and embrace the future of electronics with nanoscience as your guide.

ZEISS

Seeing beyond

WILEY

ADVANCED FUNCTIONAL MATERIALS
www.afm-journal.de

New Polymerized Small Molecular Acceptors with Non-Aromatic π-Conjugated Linkers for Efficient All-Polymer Solar Cells

Zhe Zhang, Zhixiang Li, Peiran Wang, Hongbin Chen, Kangqiao Ma, Yunxin Zhang, Tainan Duan, Chenxi Li, Zhaoyang Yao, Bin Kan, Xiangjian Wan, and Yongsheng Chen**

Developing new polymerized small molecular acceptor (PSMA) is pivotal for improving the performance of all-polymer solar cells. On the basis of this newly developed CH-series small molecule acceptors, two PSMAs are reported herein (namely PZC16 and PZC17, respectively). To reduce the molecular torsion caused by the traditional aromatic π-bridges, non-aromatic conjugated units (ethynyl for PZC16 and vinylene for PZC17) are adopted as the linkers and their effect on the photo-physical properties as well as the device performance are systematically investigated. Both polymer acceptors exhibit co-planar molecular conformation, along with broad absorption ranges and suitable energy levels. In comparison with the PM6:PZC16 film, the PM6:PZC17 film exhibits more uniform phase separation in morphology with a distinct bi-continuous network and better crystallinity. The PM6:PZC17-binary-based devices exhibit a satisfactory PCE of 16.33%, significantly higher than 9.22% of the PZC16-based devices. Impressively, PM6:PZC17-based large area device (ca. 1 cm^2) achieves an excellent PCE of 15.14%, which is among the top performance for reported all-polymer solar cells (all-PSCs).

1. Introduction

In recent years, all-polymer solar cells (all-PSCs), composed of a *p*-type polymer electron donor and an *n*-type polymer electron acceptor, have drawn tremendous attention because of their outstanding mechanical flexibility, and excellent morphological and thermal stability.[1–5] Despite of these impressive merits, the power conversion efficiencies (PCEs) of all-PSCs lag far behind the small-molecule acceptor-(SMA) based solar cells.[6–8] To overcome the shortcomings of traditional donor-acceptor polymer acceptors (low extinction coefficient, strong crystallization tendency, etc),[9–20] Li et al. proposed a creative strategy by polymerizing the acceptor-donor-acceptor (A-D-A) type SMA (PSMAs) with conjugated linkers.[21] The resulting polymer acceptors combine the merits of A-D-A SMAs as well as the polymers and consequently exhibit easily tunable absorption range and energy levels, excellent film quality, and mechanical flexibility.[4,22–23] After the emergence of Y6, the state-of-the-art PSMAs based on Y-series acceptors have witnessed the great improvements in PCEs (surpassing 17%) for binary devices.[8] Since SMA is the main building block of the PSMAs, its properties strongly affect the performance of the corresponding PSMAs. Therefore, it is pivotal to develop novel SMAs with excellent photovoltaic properties.

In our recent work, a series of highly efficient A-D-A structured SMAs (namely CH-series) has been rationally constructed,[24–26] which features a π extension in direction of the central core with respect to the Y6 series. The enhanced conjugation extension in CH-series molecules enables a much more effective and compact 3D molecular packing, which leads to improved charge transport, alleviated non-radiative recombination, and reduced E_{loss}, and thus outstanding PCEs over 18%. Their unique characters inspire us to explore their potential in constructing PSMAs. Other than SMA part, linkers also need to be carefully considered in order to obtain efficient PSMAs. Thus far, representative PSMAs usually adopt aromatic π-bridges,[27–29] such as thiophene, bithiophene, and selenophene units. Meanwhile, these aromatic π-bridges

Z. Zhang, Z. Li, P. Wang, H. Chen, K. Ma, C. Li, Z. Yao, X. Wan, Y. Chen
State Key Laboratory and Institute of Elemento-Organic Chemistry
The Centre of Nanoscale Science and Technology
and Key Laboratory of Functional Polymer Materials
Renewable Energy Conversion and Storage Center (RECAST)
College of Chemistry
Nankai University
Tianjin 300071, China
E-mail: yschen99@nankai.edu.cn

Y. Zhang, B. Kan
School of Materials Science and Engineering, National Institute for Advanced Materials
Nankai University
Tianjin 300350, China
E-mail: kanbin04@nankai.edu.cn

T. Duan
Chongqing Institute of Green and Intelligent Technology
Chongqing School
University of Chinese Academy of Sciences (UCAS Chongqing)
Chinese Academy of Sciences
Chongqing 400417, China

The ORCID identification number(s) for the author(s) of this article can be found under https://doi.org/10.1002/adfm.202214248.

DOI: 10.1002/adfm.202214248

could introduce some intramolecular twisting between linker and terminal group, which would further cause the disorder of polymer backbone orientation, and weaken the molecular packing and crystallinity of the PSMAs. As an alternative, the non-aromatic ethynyl or vinylene unit could help PSMA to achieve better coplanarity and rigid conformation,[30–34] in favor of obtaining narrow bandgaps and good charge transporting. For example, Yan et al. recently reported a vinylene-based polymer acceptor (PY-V-γ),[29] which exhibited less twisting between the end group and the linkers, better intramolecular conjugation, and tighter inter-chain packing. As a result, the vinylene-based PSMA offered a better PCE compared to its thiophene-based counterpart.

With these in mind, two new PSMAs based on a CH-series SMA were designed and synthesized, named PZC16 and PZC17, which contained ethynyl and vinylene linkers, respectively. Both PSMAs exhibited negligible twists between the terminal group and the linkers, and thus good co-planarity of the conjugated backbones. While the non-aromatic linkers slightly affected the light absorption and energy levels of PSMA, they significantly impacted the miscibility when blending with the polymer donor PM6. Compared with PZC17, the poor miscibility between PZC16 and PM6 resulted in large phase separation of the blend film, which led to inferior carrier transport. Consequently, the PM6:PZC16-based devices exhibited a low PCE of 9.22% with an open-circuit voltage (V_{oc}) of 0.859 V, short-circuit current density (J_{sc}) of 19.14 mA cm^{-2}, and fill factor (FF) of 55.75%. As a contrast, PM6:PZC17-based devices exhibited a high PCE of 16.33% with simultaneously improved V_{oc} (0.926 V), J_{sc} (23.35 mA cm^{-2}), and FF (75.54%). The better photovoltaic performance of PZC17-based device was benefitted from its more efficient exciton dissociation, faster charge transportation, less charge recombination, and reduced energy loss. Besides, PZC17-based large-area device (1 cm^2) obtained a high PCE of 15.14% which is among the best performance of the reported large-area all-PSCs. These results demonstrate the potential of CH-series SMAs and the importance of non-aromatic linkers in designing high-performance PSMAs.

2. Results and Discussion

2.1. Materials and Characterization

The chemical structures of PZC16 and PZC17 are depicted in **Figure 1**, and their detailed synthetic routes are displayed in Scheme S1 (Supporting Information). The key intermediate 2 was prepared according to our previous reports.[24–26] Then, the Konevenagel condensation of compound 3 with 2-(5-bromo-3-oxo-2,3-dihydro-1H-inden-1-ylidene)malononitrile (IC-Br) afforded compound 4 with a high yield. The commercial monobrominated terminal unit (IC-Br) without isomer was evidenced by ^{1}H NMR spectrum[35] (Figure S17, Supporting Information). Lastly, PZC16 and PZC17 were obtained by copolymerizing compound 4 with ethynyl and vinylene via the Stille coupling reaction, respectively. The number-average molecular weights of PZC16 and PZC17 were 12.0 and 7.8 KDa with a polydispersity (PDI) index of 1.68 and 1.53, respectively. Both polymer

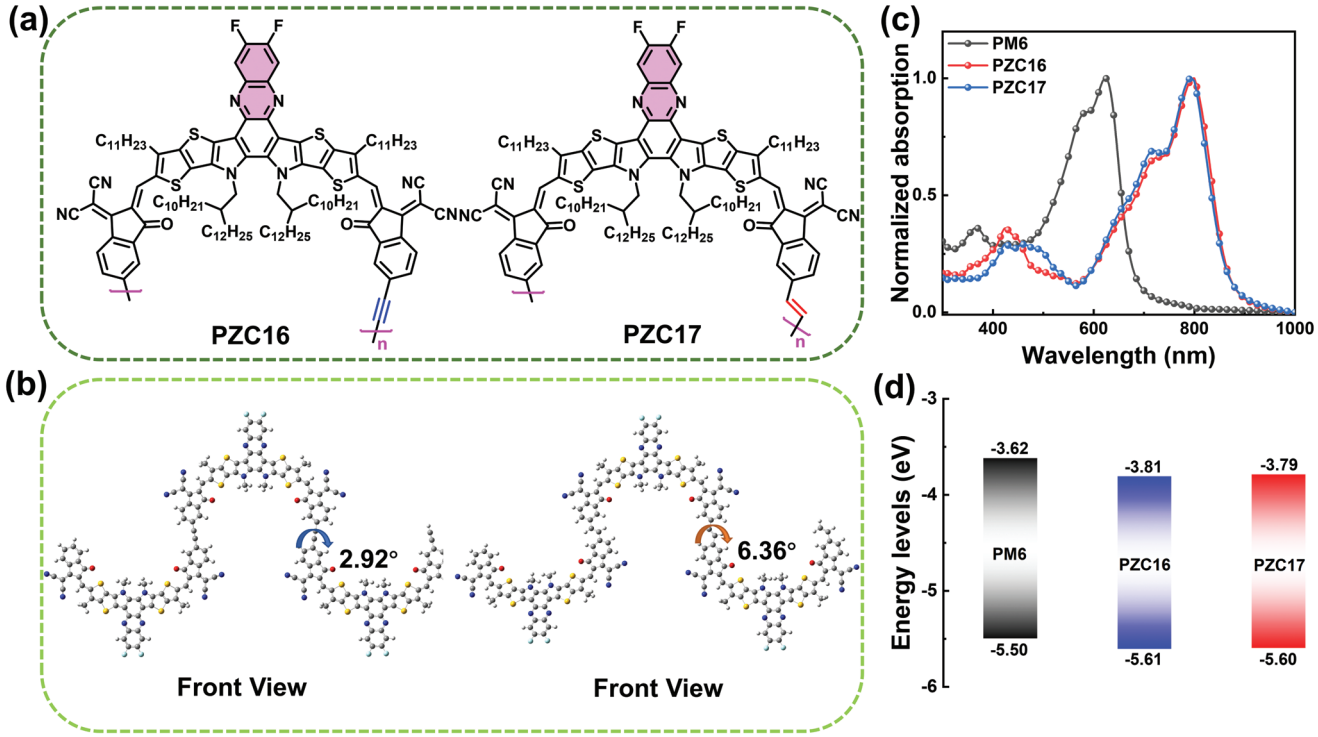

Figure 1. a) The molecular structures of PZC16 and PZC17, respectively; b) The calculated optimized trimers structures of PZC16 and PZC 17 in front view (the dihedral angle between two adjacent terminal groups); c) The normalized absorption spectra of PM6, PZC16, and PZC17 in neat film; d) The energy level diagrams of PM6, PZC16, and PZC17.

acceptors can be easily dissolved in chloroform (CF) and chlorobenzene (CB) which guarantees the solution-processability. Revealed by the density of functional theory (DFT) calculations (Figure 1b), the dihedral angle between two adjacent terminal groups is quite small (2.92° for PZC16 and 6.36° for PZC17, respectively), which is consistent with the expectation. Besides, the thermogravimetric analyses (TGA) demonstrate that both PZC16 and PZC17 exhibit good thermal stability with decomposition temperatures of 355 and 344 °C (Figure S1, Supporting Information), respectively.

2.2. Optical Properties and Energy Levels

UV–vis absorption spectra of PZC16 and PZC17 in diluted chloroform solutions and neat films were measured (Figure S2, Supporting Information; Figure 1c), and the corresponding optical and electrochemical parameters were summarized in **Table 1**. PZC16 and PZC17 display similar absorption profiles in solution with the different maximum absorption peaks located at 776 and 765 nm, respectively, which can be attributed to the more electron-deficient property of ethynyl group. In neat film, PZC16 displays a main absorption peak of 799 nm, while the absorption maximum of PZC17 locates at 793 nm. Compared with PZC16, PZC17 shows larger degree of red-shift from the solution state to the film state, implying that the existence of more condensed aggregation and stronger intermolecular interaction. To further investigate the molecular aggregation of these two polymers, their temperature-dependent UV–vis absorption spectra were measured. As shown in Figure S2 (Supporting Information), the main absorption peak of PZC16 and PZC17 both blue-shifted for only ca. 5 nm from 20 to 100 °C.[22,36] This indicates that their polymer chains are rigid and experience negligible disaggregation upon heating.[29]

The frontier orbital energy levels of both polymer acceptors were measured by cyclic voltammetry (CV) (Figure S3, Supporting Information). The highest occupied molecular orbital (HOMO) and the lowest unoccupied molecular orbital (LUMO) energy levels of PZC16 were estimated to be −5.61 and −3.81 eV, respectively. Due to the slightly enhanced electron-donating property of vinylene unit, PZC17 shows a little up-shifted HOMO and LUMO energy levels of −5.60 and −3.79 eV, respectively. The energy level diagrams of PZC16, PZC17, and PM6 are displayed in Figure 1d. It can be seen that these polymer acceptors can be well-matched with polymer donor PM6 in terms of the energy levels. The calculated HOMO/LUMO levels were −5.53/−3.50 eV for PZC16 and −5.50/−3.46 eV for PZC17, respectively (Figure S4, Supporting Information), which are consistent with the experimental results.

2.3. Photovoltaic Properties

To evaluate the photovoltaic performance of two polymer acceptors, all-PSCs were fabricated with the conventional structure of ITO/PEODT:PSS/active layers/PNDIT-F3N/Ag (**Figure 2**a), in which PM6 was used as the electron donor.[37] The current density-voltage (*J*–*V*) curves of their optimal all-PSCs devices are displayed in Figure 2b, and the corresponding photovoltaic data were summarized in **Table 2**. The variation of linkers in PZC16 and PZC17 (ethynyl vs vinylene) leads to their distinct device performance (Tables S1–S8, Supporting Information). The PZC16-based device yields a moderate PCE of 9.22% with a V_{oc} of 0.861 V, a J_{sc} of 18.98 mA cm^{-2}, and an FF of 56.65%. As a contrast, the PZC17-based device demonstrates essentially enhanced V_{oc}, J_{sc}, and FF, which are 0.926 V, 23.35 mA cm^{-2}, and 75.54%, respectively. As a result, a high PCE of 16.33% was realized by the PZC17-based device. To our knowledge, this result with efficiency over 16% represents very few polymer acceptors featured with new SMA units. In addition, the thermal stability of the PM6:PZC17-based devices was characterized under continuous heating of 65 °C without encapsulation in the nitrogen-filled glove box. As shown in Figure S5 (Supporting Information), PZC17-based device maintains 74% of its initial PCE after 300 h, suggesting its satisfactory thermal stability. To demonstrate the potential of PZC-17 in fabricating large-area devices, all-PSCs with an effective area of 1 cm^2 were fabricated. The resultant device achieved an excellent PCE of 15.14% (Figure 2d), which is, to our knowledge, one of the highest values reported[28,38–39] for all-PSCs with a device area as large as 1 cm^2, suggesting its capability for practical applications.

External quantum efficiency (EQE) spectra of the PZC16 and PZC17-based devices were recorded to verify their quite different J_{sc} values. As shown in Figure 2c, though both devices show similar and broad photo-response from 300 to 900 nm, the PZC17-based device displays much higher EQE response with a maximum EQE value of 85% compared with the PZC16-based device in the range of 350–850 nm, indicating more efficient photon-electron conversion for PZC17-based device. The integrated J_{sc} calculated from the EQE spectra was 19.29 mA cm^{-2} for PZC16-based device and 23.04 mA cm^{-2} for PZC17-based device, respectively, which are fairly consistent with the J_{sc} values obtained from their *J*–*V* curves.

2.4. Charge Dynamic Investigation

To investigate the exciton dissociation process in the blend films of PM6:PZC16 and PM6:PZC17, steady-state photoluminescence (PL) spectroscopy was performed. As can be seen in Figure S6 (Supporting Information), the PL quenching efficiency of donor was calculated to be 96.5% in the PM6:PZC16 blend,

Table 1. Summary of the physicochemical features of PZC16 and PZC17.

Comp	λsol max [nm]	λfilm max [nm]	λfilm edge [nm]	Eonset g[eV]	HOMOa) [eV]	LUMOa) [eV]	HOMOb) [eV]	LUMOb) [eV]
PZC16	776	799	868	1.43	−5.53	−3.50	−5.61	−3.81
PZC17	765	793	864	1.44	−5.50	−3.46	−5.60	−3.79

a)Calculated by the DFT simulations; b)Obtained from CV.

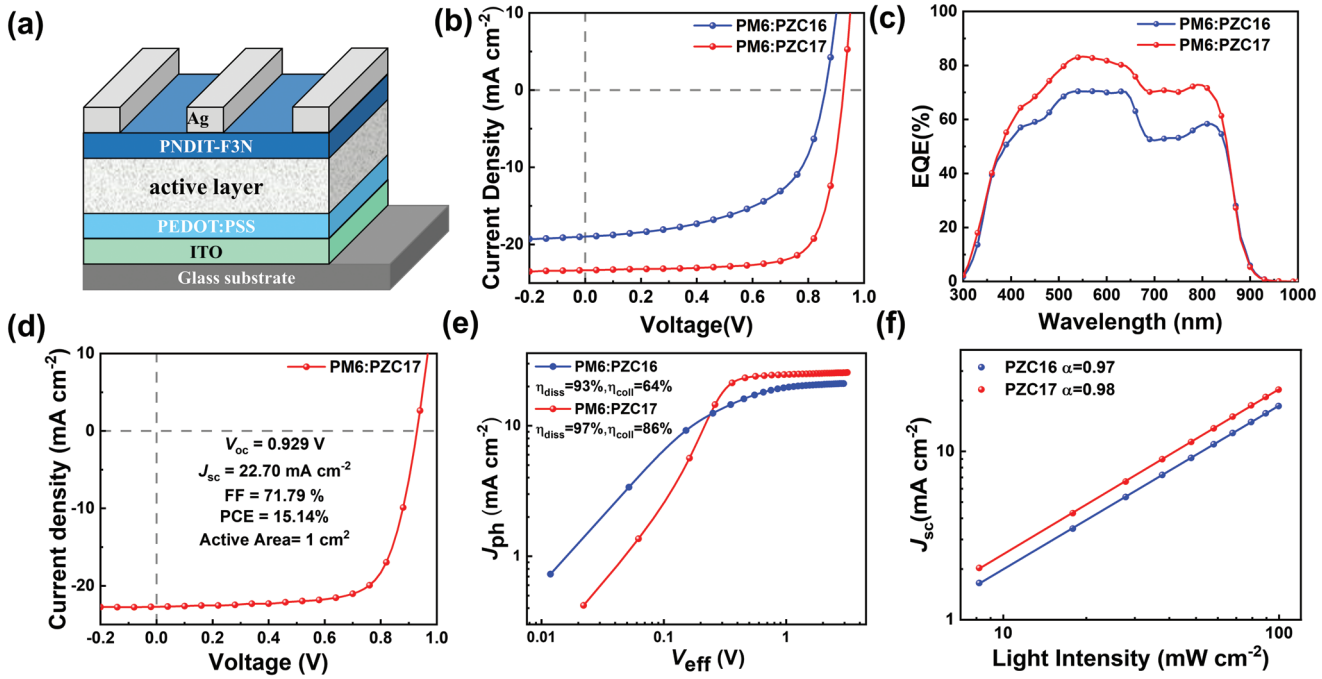

Figure 2. a) Device architecture of all-PSCs; b) *J*--*V* curves and c) EQE spectra of the all-PSCs; d) *J*–*V* curve of PM6:PZC17-based device with an active area of 1 cm^2; e) J_{ph}–V_{eff} curves of PM6:PZC16 and PM6:PZC17 blend films; f) J_{sc} versus light intensity of PM6:PZC16 and PM6:PZC17.

and 96.9% in the PM6:PZC17 blend, respectively. The PL quenching efficiency of acceptor was 80.0% in the PM6:PZC17 blend, which was higher than that of PM6:PZC16(68.8%). Overall, PL results indicate that more efficient exciton dissociation occurred in the PM6:PZC17 blend, which is consistent with the increased J_{sc} value in devices. To better understand the disparity in photovoltaic performance of two PSMAs, the dependence of the photocurrent density (J_{ph}) on the effective voltage (V_{eff}) was measured (Figure 2e).[40] The exciton dissociation efficiency (η_{diss}) and charge collection efficiency (η_{coll}) can be assessed from the ratio of J_{ph}/J_{sat} under the short-circuit condition and maximum power output point, respectively. Accordingly, the η_{diss}/η_{coll} are calculated to be 97.03%/85.71% for the PZC17-based device, higher than those for the PZC16-based device, indicating more efficient charge generation and collection process in the PZC17-based device. The dependence of J_{sc} on light density was further measured to investigate the bimolecular recombination in both optimal devices.[41] The relation between the J_{sc} and the P_{light} (light density) can be described by the equation: $J_{sc} \propto P_{light}^{S}$. As displayed in Figure 2f, the *S* values obtained by fitting J_{sc} as a function of the light density are 0.97 for the PZC16-based devices and 0.98 for the PZC17-based devices, respectively. The *S* value of the PZC17-based device is closer to 1, indicating less bimolecular recombination in the corresponding device. Besides, the PZC17-based device exhibits less trap-assisted recombination as revealed by investigating the relationship between the V_{oc} and the P_{light} (Figure S7, Supporting Information).

Table 2. Summary of photovoltaic parameters of all-PSCs.

Active layer	V_{oc} [V]	J_{sc} [mA cm^{-2}]	FF [%]	PCE [%]
PM6:PZC16	0.861	18.98	56.65	9.22
	(0.862 ± 0.0003)	(19.06 ± 0.16)	(55.69 ± 0.82)	(9.16 ± 0.06)
PM6:PZC17	0.926	23.35	75.54	16.33
	(0.925 ± 0.0003)	(23.38 ± 0.08)	(75.19±0.30)	(16.26 ± 0.04)
PM6:PZC17[a)]	0.929	22.70	71.79	15.14

[a)]all-PSCs with 1 cm^2 active area. The average parameters were calculated from 15 independent devices.

The transient photocurrent (TPC) and the transient photovoltage (TPV) characterizations were performed to investigate the charge extraction and recombination process in all-PSCs devices (Figure S8, Supporting Information). Compared with the PZC16-based device, the PZC17-based device demonstrates a faster charge extraction time of 0.30 µs. Meanwhile, the longer carrier lifetime of 9.2 µs observed in the PZC17-based device suggests its weaker charge recombination behaviors.[22,42,43] Space charge-limited current (SCLC) method was used to evaluate their charge transport abilities (Figures S9 and S10, Supporting Information). The electron mobility (μ_e) of PZC17 neat film (5.54×10^{-4} cm^2 V^{-1} s^{-1}) is larger than that of PZC16 (3.85×10^{-4} cm^2 V^{-1} s^{-1}), which is consistent with its tighter smaller π-π stacking distance and larger crystal coherence lengths (CCLs) as revealed by the grazing incidence wide-angle X-ray scattering (GIWAXS) results. The electron mobility (μ_e) and the hole mobility (μ_h) of the PM6:PZC16 blend film were estimated to be 1.72×10^{-4} cm^2 V^{-1} s^{-1} and 8.55×10^{-5} cm^2 V^{-1} s^{-1}, respectively. The μ_e and μ_h of the PM6:PZC17 blend film were increased to 1.76×10^{-4} and 1.19×10^{-4} cm^2 V^{-1} s^{-1}, respectively. The higher and more balanced the μ_e/μ_h of PM6:PZC17 blend film is beneficial to the charge extraction and collection.[44] The above analyses reveal

the facts that more efficient charge generation, faster charge transport, and less charge recombination occurred in the PZC17-based device, which improved its J_{sc} and FF values.

2.5. Morphology Analysis

The atomic force microscopy (AFM) was used to investigate the effect of different linkers on the morphological characteristics of blend films. As illustrated in **Figure 3**a,d, compared with the PM6:PZC16 blend film, the PM6:PZC17 film shows smoother surface with a smaller value of root-mean-square (RMS) roughness of 1.49 nm. The smoother surface could favor the contact between the interfacial layer and active layer. As presented in the AFM phase images (Figure S11, Supporting Information), the PM6:PZC17 blend film shows a smaller and more uniform phase separation morphology with a more distinct bi-continuous network,[45] which is beneficial for exciton dissociation and charge transportation. In order to better understand the difference in the morphology of the active layer, the contact-angle measurements of the neat films were carried out to estimate the Flory–Huggins interaction parameters χ.[46–48] The χ is calculated by the equation: $\chi = K(\sqrt{\gamma_d} - \sqrt{\gamma_a})^2$, where K is a constant, γ_d is the surface energy of the polymer donor and γ_a is the surface energy of the polymer acceptor. A higher value of χ, meaning lower miscibility of donor and acceptor, would usually result in larger size phase separations. As shown in Table S9 (Supporting Information), the smaller χ value (0.18 K) between PM6 and PZC17 (0.47 K for PM6 and PZC16) demonstrates a higher miscibility of PM6 and PZC17, likely leading to a more suitable size phase separation, which is also consistent with the results of the AFM.

Besides, the crystallization and orientation of polymer chains also considerably affect exciton dissociation and charge transport in devices. Therefore, the grazing incidence wide-angle X-ray scattering (GIWAXS) measurement was further conducted to provide structural information of the blend films.[49–51] The 2D patterns of the neat films are presented in Figure S12 (Supporting Information) and the 1D extracted profiles of the neat film are shown in Figure 3c. Clear (010) diffraction peak in the out-of-plane (OOP) direction and (100) diffraction peak in the in-plane (IP) direction were observed in both the PZC16 and PZC17 neat film, implying their preferred face-on molecular orientations. The (010) peaks of PZC16 and PZC17 films located at q = 1.62 Å^{-1} and q = 1.65 Å^{-1}, indicating the corresponding π-π stacking distance of 3.88 and 3.81 Å, respectively (Table S10, Supporting Information). Besides, the CCLs of (010) orientation, which can be calculated by the Scherrer equation, are 14.2 Å for PZC16 and 20.9 Å for PZC17, respectively. The smaller $d_{\pi\text{-}\pi}$ along with larger CCL of PZC17 would indisputably facilitate the charge transportation. After blending with PM6, both blend films still exhibit more dominant face-on orientations, as evidenced by the clear (010) diffraction peak in the OOP direction and (100) peak in the IP direction. In the OOP direction, both blend films exhibit similar π-π stacking distances (3.70 Å for PM6:PZC16, 3.69 Å for PM6:PZC17), which is consistent with the π-π stacking distances of PM6 in neat films (3.69 Å). In addition, in comparison with the PM6:PZC16 blend film, the PM6:PZC17 blend film shows a larger CCL of (010) peak region in the OOP and IP direction, further indicating its better charge transporting properties.

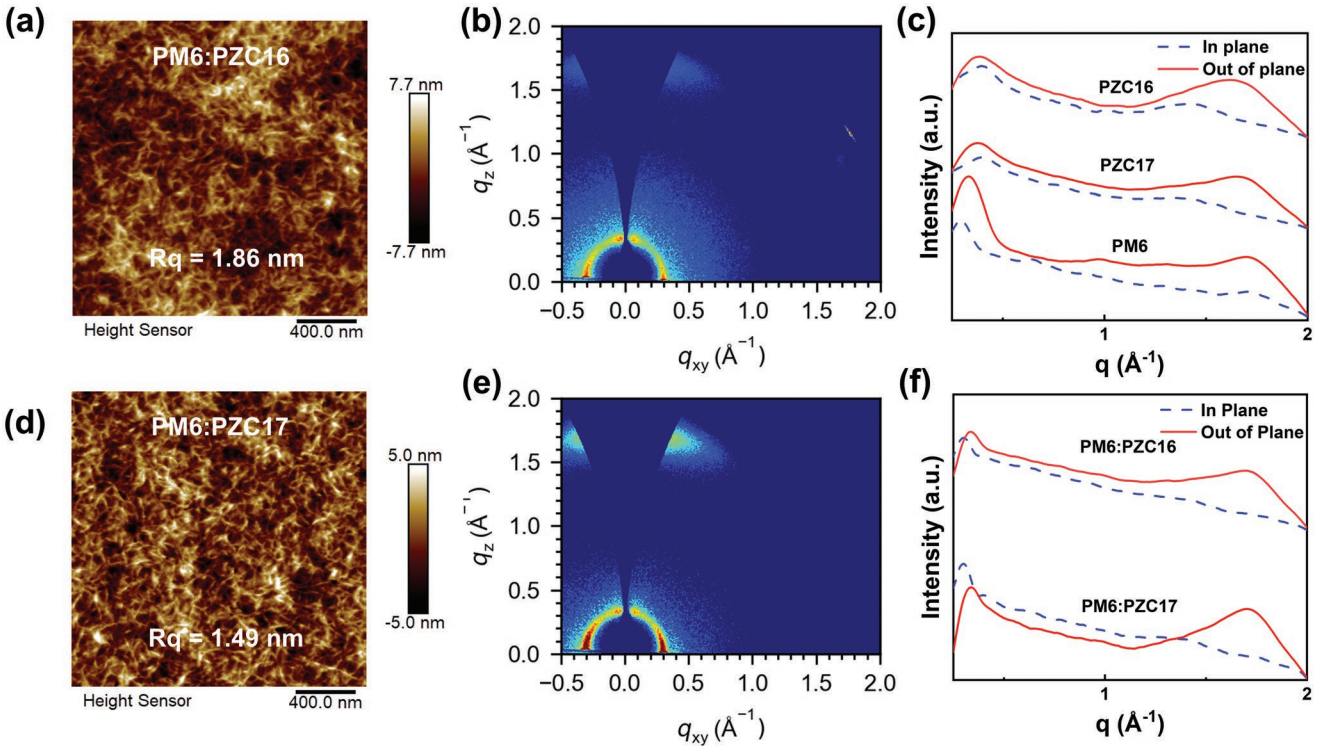

Figure 3. a,d) AFM height images of PM6:PZC16 and PM6:PZC17; b,e) 2D GIWAXS patterns of the optimized blend films of PM6:PZC16 and PM6:PZC17; c,f) Line cuts of GIWAXS images of the neat films and the blend films.

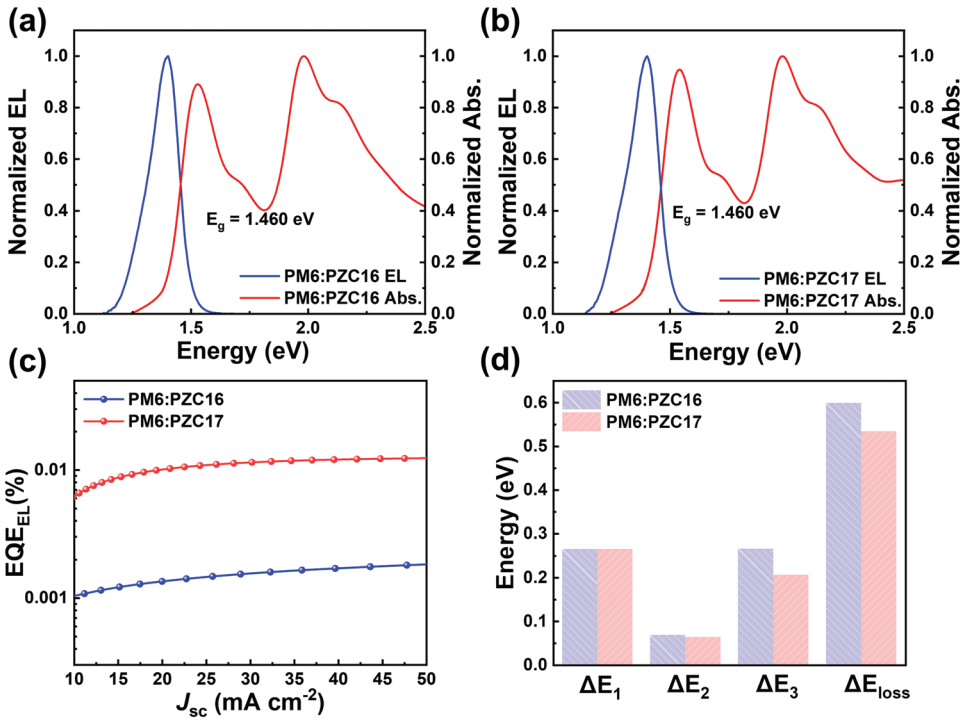

Figure 4. a,b) Normalized optical absorption and EL spectra of PM6:PZC16 and PM6:PZC17; c) EL quantum efficiencies of PM6:PZC16 and PM6:PZC17 under different injected current densities; d) E_{loss} and its detailed three parts of ΔE_1, ΔE_1, and ΔE_3 values.

2.6. Energy Loss Analysis

Large energy loss severely limits the efficiency of organic solar cells. Hence, the detailed energy loss analysis was conducted to quantify the voltage loss in two PSMAs-based devices (**Figure 4**). The band gaps (E_g) of two blend films, determined by the crossing point between optical absorption and electroluminescence (EL) spectra of the blend film,[28,52] are ≈1.460 eV. The energy loss in the first part of two polymer acceptors-based devices is same (0.265 eV) due to their identical E_g. The second part (ΔE_2) of the PM6:PZC16-based device was calculated to be 0.068 eV, which is slighlty larger than 0.063 eV for the PM6:PZC17-based device. Meanwhile, the PM6:PZC17-based device shows a higher EQE_{EL} of 1.09×10^{-4} compared to the PM6:PZC16-based device with the EQE_{EL} of 1.3×10^{-5}. The corresponding ΔE_3 were estimated to be 0.291 and 0.236 eV for the PM6:PZC16-based devices and the PM6:PZC17-based devices, respectively, similar to those determined from the sensitive EQE measurements (**Table 3**). Therefore, the higher V_{oc} of the PM6:PZC17-based devices can be attributed to the decreased radiative recombination loss and non-radiative recombination loss.

3. Conclusion

In summary, we reported two PSMAs constructed with a new SMA along with different non-aromatic linkers. The non-aromatic linkers enabled good coplanarity and intramolecular conjugation. Compared with PZC17, PZC16 showed slightly red-shifted and down-shifted energy which can be ascribed to the electron-withdrawing property of ethynyl unit. However, the PM6:PZC16-based device gave an inferior PCE of 9.22%. The morphology analysis revealed that the poor miscibility between PM6 and PZC16 led to the oversized phase segregation which resulted in unfavorable exciton dissociation and charge transport, severe charge recombination, and large energy loss for the corresponding all-PSC devices. On the contrary, the PM6:PZC17-based device achieved more suitable phase separation and exhibited simultaneously improved V_{oc} of 0.926 V, J_{sc} of 23.35 mA cm^{-2}, and FF of 75.54%, which led to an impressive PCE of 16.33%. Moreover, the PM6:PZC17-based large-area device of 1 cm^2 also achieved an excellent PCE of 15.14%, which represents one of the best results for all-polymer large-area devices. Our work highlights the great potential of CH-series

Table 3. Total energy loss values and different contributions in organic solar cells based on the SQ limit theory.

Device	E_g[a)] [eV]	V_{oc} [V]	$V_{oc,sq}$[b)] [V]	$V_{oc,rad}$[c)] [V]	ΔE_1 [eV]	ΔE_2 [eV]	ΔE_3[d)] [eV]	ΔE_3[e)] [eV]	E_{loss} [eV]
PM6:PZC16	1.460	0.861	1.195	1.127	0.265	0.068	0.266	0.291	0.599
PM6:PZC17	1.460	0.926	1.195	1.132	0.265	0.063	0.206	0.236	0.534

[a)] E_g was determined by the crossing point between optical absorption and EL spectra of the blend film; [b)] $V_{oc,sq}$ is calculated according to the SQ limit; [c)] $V_{oc,rad}$ is the V_{oc} when there is only radiative recombination and is calculated from the EQE, FTPS-EQE, and EL measurements; [d)] ΔE_3 was calculated by $q(V_{oc,rad}\text{-}V_{oc})$; [e)] ΔE_3 was obtained from the equation $q\Delta V_{nr} = -kT\ln EQE_{EL}$ by measuring the device EQE_{EL}.

SMAs and the importance of non-aromatic linkage units in constructing high-performance PSMAs.

Supporting Information

Supporting Information is available from the Wiley Online Library or from the author.

Acknowledgements

Z.Z and Z.L. contributed equally to this work. The authors gratefully acknowledge the financial support from NSFC (21935007 and 52025033) and MoST (2022YFB4200400 and 2019YFA0705900) of China, Tianjin city (20JCZDJC00740), 111 Project (B12015), the 100 Young Academic Leaders Program of Nankai University (020-ZB22000110), the Fundamental Research Funds for the Central Universities, Nankai University (023-ZB22000105), Haihe Laboratory of Sustainable Chemical Transformations. A portion of this work is based on the data obtained at BSRF-1W1A. The authors gratefully acknowledge the cooperation of the beamline scientists at BSRF-1W1A beamline.

Conflict of Interest

The authors declare no conflict of interest.

Data Availability Statement

The data that support the findings of this study are available from the corresponding author upon reasonable request.

Keywords

all-polymer solar cells, ethynyl units, polymer acceptors, power conversion efficiencies, vinyl units

Received: December 6, 2022
Revised: February 9, 2023
Published online: March 4, 2023

[1] S. Ma, H. Zhang, K. Feng, X. Guo, *Chem. - Eur. J.* **2022**, *28*, 202200222.
[2] H. Yin, C. Yan, H. Hu, J. K. W. Ho, X. Zhan, G. Li, S. K. So, *Mater. Sci. Eng. R Rep.* **2020**, *140*, 100542.
[3] G. Wang, F. S. Melkonyan, A. Facchetti, T. J. Marks, *Angew. Chem., Int. Ed.* **2019**, *58*, 4129.
[4] Z. G. Zhang, Y. Li, *Angew. Chem., Int. Ed.* **2021**, *60*, 4422.
[5] M. Kataria, H. D. Chau, N. Y. Kwon, S. H. Park, M. J. Cho, D. H. Choi, *ACS Energy Lett.* **2022**, *7*, 3835.
[6] L. Zhu, M. Zhang, J. Xu, C. Li, J. Yan, G. Zhou, W. Zhong, T. Hao, J. Song, X. Xue, Z. Zhou, R. Zeng, H. Zhu, C. C. Chen, R. C. I. MacKenzie, Y. Zou, J. Nelson, Y. Zhang, Y. Sun, F. Liu, *Nat. Mater.* **2022**, *21*, 656.
[7] Y. Cui, Y. Xu, H. Yao, P. Bi, L. Hong, J. Zhang, Y. Zu, T. Zhang, J. Qin, J. Ren, Z. Chen, C. He, X. Hao, Z. Wei, J. Hou, *Adv. Mater.* **2021**, *33*, 2102420.
[8] J. Wang, Y. Cui, Y. Xu, K. Xian, P. Bi, Z. Chen, K. Zhou, L. Ma, T. Zhang, Y. Yang, Y. Zu, H. Yao, X. Hao, L. Ye, J. Hou, *Adv. Mater.* **2022**, *34*, 2205009.
[9] X. Zhan, Z. A. Tan, B. Domercq, Z. An, X. Zhang, S. Barlow, Y. Li, D. Zhu, B. Kippelen, S. R. Marder, *J. Am. Chem. Soc.* **2007**, *129*, 7246.
[10] Z. A. Tan, E. Zhou, X. Zhan, X. Wang, Y. Li, S. Barlow, S. R. Marder, *Appl. Phys. Lett.* **2008**, *93*, 073309.
[11] H. Yan, Z. Chen, Y. Zheng, C. Newman, J. R. Quinn, F. Dotz, M. Kastler, A. Facchetti, *Nature* **2009**, *457*, 679.
[12] C. Mu, P. Liu, W. Ma, K. Jiang, J. Zhao, K. Zhang, Z. Chen, Z. Wei, Y. Yi, J. Wang, S. Yang, F. Huang, A. Facchetti, H. Ade, H. Yan, *Adv. Mater.* **2014**, *26*, 7224.
[13] Z. Li, W. Zhong, L. Ying, F. Liu, N. Li, F. Huang, Y. Cao, *Nano Energy* **2019**, *64*, 103931.
[14] M. F. Falzon, A. P. Zoombelt, M. M. Wienk, R. A. Janssen, *Phys. Chem. Chem. Phys.* **2011**, *13*, 8931.
[15] R. Stalder, J. Mei, J. Subbiah, C. Grand, L. A. Estrada, F. So, J. R. Reynolds, *Macromolecules* **2011**, *44*, 6303.
[16] S. Liu, Z. Kan, S. Thomas, F. Cruciani, J. L. Bredas, P. M. Beaujuge, *Angew. Chem., Int. Ed.* **2016**, *55*, 12996.
[17] H. Sun, Y. Tang, C. W. Koh, S. Ling, R. Wang, K. Yang, J. Yu, Y. Shi, Y. Wang, H. Y. Woo, X. Guo, *Adv. Mater.* **2019**, *31*, 1807220.
[18] C. Dou, Z. Ding, Z. Zhang, Z. Xie, J. Liu, L. Wang, *Angew. Chem., Int. Ed.* **2015**, *54*, 3648.
[19] S. Shi, P. Chen, Y. Chen, K. Feng, B. Liu, J. Chen, Q. Liao, B. Tu, J. Luo, M. Su, H. Guo, M. G. Kim, A. Facchetti, X. Guo, *Adv. Mater.* **2019**, *31*, 1905161.
[20] X. Long, Z. Ding, C. Dou, J. Zhang, J. Liu, L. Wang, *Adv. Mater.* **2016**, *28*, 6504.
[21] Z. G. Zhang, Y. Yang, J. Yao, L. Xue, S. Chen, X. Li, W. Morrison, C. Yang, Y. Li, *Angew. Chem., Int. Ed.* **2017**, *56*, 13503.
[22] J. Du, K. Hu, J. Zhang, L. Meng, J. Yue, I. Angunawela, H. Yan, S. Qin, X. Kong, Z. Zhang, B. Guan, H. Ade, Y. Li, *Nat. Commun.* **2021**, *12*, 5264.
[23] B. Kan, X. Wan, C. Li, Y. Chen, *Acta Polym. Sin.* **2021**, *52*, 1262.
[24] H. Chen, H. Liang, Z. Guo, Y. Zhu, Z. Zhang, Z. Li, X. Cao, H. Wang, W. Feng, Y. Zou, L. Meng, X. Xu, B. Kan, C. Li, Z. Yao, X. Wan, Z. Ma, Y. Chen, *Angew. Chem., Int. Ed.* **2022**, *61*, 202209580.
[25] Y. Zou, H. Chen, X. Bi, X. Xu, H. Wang, M. Lin, Z. Ma, M. Zhang, C. Li, X. Wan, G. Long, Y. Zhaoyang, Y. Chen, *Energy Environ. Sci.* **2022**, *15*, 3519.
[26] H. Chen, Y. Zou, H. Liang, T. He, X. Xu, Y. Zhang, Z. Ma, J. Wang, M. Zhang, Q. Li, C. Li, G. Long, X. Wan, Z. Yao, Y. Chen, *Sci. China: Chem.* **2022**, *65*, 1362.
[27] Q. Wu, W. Wang, Y. Wu, R. Sun, J. Guo, M. Shi, J. Min, *Natl. Sci. Rev.* **2022**, *9*, nwab151.
[28] Q. Fan, H. Fu, Q. Wu, Z. Wu, F. Lin, Z. Zhu, J. Min, H. Y. Woo, A. K. Jen, *Angew. Chem., Int. Ed.* **2021**, *60*, 15935.
[29] H. Yu, Y. Wang, H. K. Kim, X. Wu, Y. Li, Z. Yao, M. Pan, X. Zou, J. Zhang, S. Chen, D. Zhao, F. Huang, X. Lu, Z. Zhu, H. Yan, *Adv. Mater.* **2022**, *34*, 2200361.
[30] Y. Wang, Q. Liao, G. Wang, H. Guo, X. Zhang, M. A. Uddin, S. Shi, H. Su, J. Dai, X. Cheng, A. Facchetti, T. J. Marks, X. Guo, *Chem. Mater.* **2017**, *29*, 4109.
[31] F. Tang, K. Wu, Z. Zhou, G. Wang, B. Zhao, S. Tan, *ACS Appl. Energy Mater.* **2019**, *2*, 3918.
[32] J. Liao, H. Zhao, Z. Cai, Y. Xu, F. G. F. Qin, Q. Zong, F. Peng, Y. Fang, *Org. Electron.* **2018**, *61*, 215.
[33] J. Liu, N. Zheng, Z. Hu, Z. Wang, X. Yang, F. Huang, Y. Cao, *Sci. China: Chem.* **2017**, *60*, 1136.
[34] Q. Bao, Q. Zhang, Y. Li, H. Li, J. He, Q. Xu, N. Li, D. Chen, J. Lu, *Org. Electron.* **2016**, *28*, 155.
[35] Z. Luo, T. Liu, R. Ma, Y. Xiao, L. Zhan, G. Zhang, H. Sun, F. Ni, G. Chai, J. Wang, C. Zhong, Y. Zou, X. Guo, X. Lu, H. Chen, H. Yan, C. Yang, *Adv. Mater.* **2020**, *32*, 2005942.
[36] R. Steyrleuthner, M. Schubert, I. Howard, B. Klaumunzer, K. Schilling, Z. Chen, P. Saalfrank, F. Laquai, A. Facchetti, D. Neher, *J. Am. Chem. Soc.* **2012**, *134*, 18303.

[37] M. Zhang, X. Guo, W. Ma, H. Ade, J. Hou, *Adv. Mater.* **2015**, *27*, 4655.
[38] J. Liu, J. Deng, Y. Zhu, X. Geng, L. Zhang, S. Y. Jeong, D. Zhou, H. Y. Woo, D. Chen, F. Wu, L. Chen, *Adv. Mater.* **2022**, *35*, 2208008.
[39] K. Xian, K. Zhou, M. Li, J. Liu, Y. Zhang, T. Zhang, Y. Cui, W. Zhao, C. Yang, J. Hou, Y. Geng, L. Ye, *Chin. J. Chem.* **2022**, *41*, 159.
[40] K. Zhang, Z. Liu, N. Wang, *J. Power Sources* **2019**, *413*, 391.
[41] S. R. Cowan, A. Roy, A. J. Heeger, *Phys. Rev. B* **2010**, *82*, 245207.
[42] Z. Wang, K. Gao, Y. Kan, M. Zhang, C. Qiu, L. Zhu, Z. Zhao, X. Peng, W. Feng, Z. Qian, X. Gu, A. K. Jen, B. Z. Tang, Y. Cao, Y. Zhang, F. Liu, *Nat. Commun.* **2021**, *12*, 332.
[43] Q. Yang, W. Yu, J. Lv, P. Huang, G. He, Z. Xiao, Z. Kan, S. Lu, *Dyes Pigm.* **2022**, *200*, 110180.
[44] C. M. Proctor, J. A. Love, T. Q. Nguyen, *Adv. Mater.* **2014**, *26*, 5957.
[45] K. Jiang, J. Zhang, Z. Peng, F. Lin, S. Wu, Z. Li, Y. Chen, H. Yan, H. Ade, Z. Zhu, A. K. Jen, *Nat. Commun.* **2021**, *12*, 468.
[46] S. Kouijzer, J. J. Michels, M. van den Berg, V. S. Gevaerts, M. Turbiez, M. M. Wienk, R. A. Janssen, *J. Am. Chem. Soc.* **2013**, *135*, 12057.
[47] J. Zhang, C. H. Tan, K. Zhang, T. Jia, Y. Cui, W. Deng, X. Liao, H. Wu, Q. Xu, F. Huang, Y. Cao, *Adv. Energy Mater.* **2021**, *11*, 2102559.
[48] D. Zhou, C. Liao, S. Peng, X. Xu, Y. Guo, J. Xia, H. Meng, L. Yu, R. Li, Q. Peng, *Adv. Sci.* **2022**, *9*, 2202022.
[49] J. L. Baker, L. H. Jimison, S. Mannsfeld, S. Volkman, S. Yin, V. Subramanian, A. Salleo, A. P. Alivisatos, M. F. Toney, *Langmuir* **2010**, *26*, 9146.
[50] A. Hexemer, W. Bras, J. Glossinger, E. Schaible, E. Gann, R. Kirian, A. MacDowell, M. Church, B. Rude, H. Padmore, *J. Phys.: Conf. Ser.* **2010**, *247*, 012007.
[51] J. Rivnay, S. C. Mannsfeld, C. E. Miller, A. Salleo, M. F. Toney, *Chem. Rev.* **2012**, *112*, 5488.
[52] Y. Wang, D. Qian, Y. Cui, H. Zhang, J. Hou, K. Vandewal, T. Kirchartz, F. Gao, *Adv. Energy Mater.* **2018**, *8*, 1801352.